Nucleic Acids Research, 2024, **52**, 10775–10787
https://doi.org/10.1093/nar/gkae754
Advance access publication date: 1 September 2024
Chemical Biology and Nucleic Acid Chemistry

Modulation of dynamic DNA G-quadruplex structures in the hTERT promoter region by ligands

Deepak Karna [1], Lin Liang[1], Grinsun Sharma[2], Shankar Mandal[1], Sefan Asamitsu[3], Yusuke Kawamoto[3], Kaori Hashiya[3], Toshikazu Bando[3], Hiroshi Sugiyama[3,4] and Hanbin Mao[1,2,*]

[1]Department of Chemistry and Biochemistry, Kent State University, Kent, OH 44242, USA
[2]School of Biomedical Science, Kent State University, Kent, OH 44242, USA
[3]Department of Chemistry, Graduate School of Science, Kyoto University, Sakyo, Kyoto 606-8502, Japan
[4]Institute for Integrated Cell–Material Science (iCeMS), Kyoto University, Sakyo, Kyoto 606-8501, Japan
*To whom correspondence should be addressed. Tel: +1 330 672 9380; Fax: +1 330 672 3816; Email: hmao@kent.edu

Abstract

Small molecules can inhibit cellular processes such as replication and transcription by binding to the promoter regions that are prone to form G-quadruplexes. However, since G-quadruplexes exist throughout the human genome, the G-quadruplex binders suffer from specificity issues. To tackle this problem, a G-quadruplex binder (Pyridostatin, or PDS) is conjugated with a ligand (Polyamide, or PA) that can specifically recognize DNA sequences flanking the G-quadruplex forming region. The binding mechanism of this hybrid ligand to the hTERT promoter region (hTERT 5–12) is then elucidated using optical tweezers. During mechanical unfolding processes, different intermediate structures of hTERT 5–12 in presence of PDS, PA, or PA-PDS conjugate are observed. These intermediate structures are consistent with two folding patterns of G-quadruplexes in the hTERT 5–12 fragment. While the duplex DNA binder PA facilitates the folding of a hairpin-G-quadruplex structure, the PDS assists the formation of two tandem G-quadruplexes. Both replication stop assay *in vitro* and dual luciferase assay *in vivo* established the effectiveness of the PA-PDS conjugate for hTERT 5–12 targeting. We expect such a ligand dependent folding dynamics will provide guidelines to the development of drugs that not only target hTERT expressions, but also other oncogenes via interactions with specific G-quadruplex structures formed in their promotor regions.

Graphical abstract

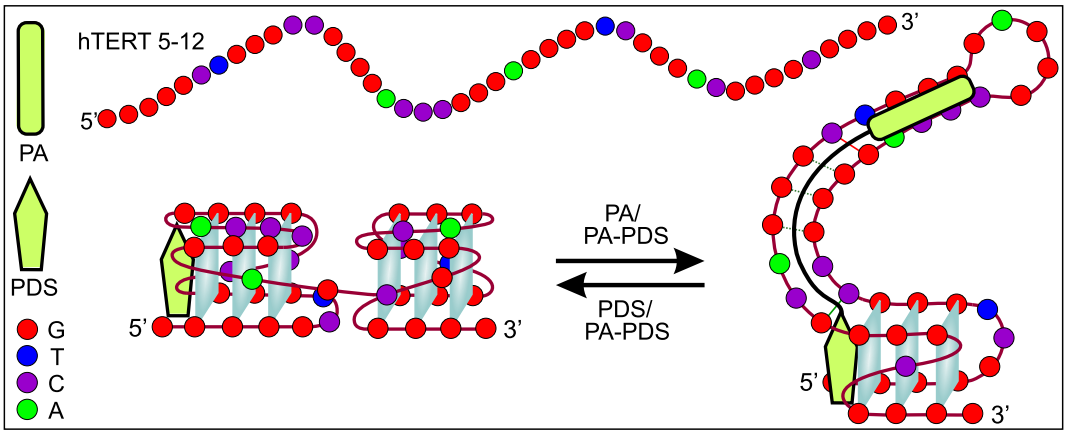

Introduction

Guanine rich sequences of DNA tend to fold into a four-stranded structure called G-quadruplex (GQ), which consists of a stack of quadrilateral G-quartet planes held by Hoogsteen hydrogen bonding among four guanine residues. Such GQs are prominently found in telomeric regions as well as in promoter regions of genes (1–4) important for initiating transcription. Although cellular transcription is a well-controlled process modulated by promoters, any irregularities during the event can cause biological abnormalities such as cancer. In majority of cancer cells, the abnormal overexpression of *TERT* gene is observed to be responsible for the production of human telomerase (5,6). Human telomerase adds telomeric DNA repeats (5′-TTAGGG) to the end of chromosome,

Received: March 24, 2023. **Revised:** July 9, 2024. **Editorial Decision:** August 15, 2024. **Accepted:** August 20, 2024

maintaining the length of telomere which leads to immortality of cancer cells. GQs are found to obstruct the replication and transcription of oncogenes. Given the complexity of human telomerase reverse transcriptase (*hTERT*) and many other promoter regions that involve GQ formation (*c-MYC*, *c-KIT*, *KRAS*, *VGEF*, *BCL-2*, *PDGF-β* etc.) (7), it is urgent to understand those complicated folding patterns in order to provide insights for more effective interventions of gene regulation through G-quadruplexes. Among several strategies to control gene regulations (8–11), one of the most studied method is usage of small molecule binders. Small molecules bound to GQs can provide additional mechanical stability, thereby inhibiting the expression of oncogenes by motor proteins such as DNA/RNA polymerases. However, most GQ ligands use generic binding mechanisms such as pi-pi stacking and electrostatic attractions to bind to G-quadruplex, causing a specificity problem. Given that approximately 716310 potential GQ forming sequences exist in human genome (12), the specificity problem is expected to be prevalent in the GQ targeting approach to fight cancers.

Previous studies have shown that pyrrole-imidazole based polyamide (PA) can bind to duplex DNA with a specific sequence (13). An antiparallel arrangement of imidazole and pyrrole can recognize G-C base pair while pyrrole-pyrrole arrangement binds to A-T or T-A base pair (14). Given that GQ forming sequence in promoter is flanked by duplex DNA segments, we reasoned that a particular promoter GQ can be recognized by specific targeting of nearby duplex DNA segments. Since pyridostatin (PDS) (15) is a well-known ligand with high affinity binding to GQs, we attached a PA moiety to the PDS to generate a new chimera ligand PA-PDS. Here, the PA-PDS conjugated by click-chemistry is designed to target the hTERT promoter region (hTERT 5–12). The hTERT 5–12 (−90 to −46) core promoter region contains eight tracts of guanine rich repeats. Several interchangeable secondary structures have been reported at this promoter site (16–19). Given these dynamic and complex structures, small molecule ligands are expected to be developed to specifically target this region for potential cancer treatment (20,21). In one model, a loop with a hairpin conformation exists in a GQ structure. A PA sequence is therefore designed to specifically bind to the duplex DNA tract inside this loop. By using this PA-PDS compound, we investigated the binding mechanism of the ligand to the hTERT 5–12 region using mechanical unfolding in optical tweezers. Although other methods such as DMS footprinting and DNase footprinting can provide a basic understanding of folding patterns in secondary and tertiary biological structures, the sensitivity of these methods makes it rather challenging to differentiate origins of pattern change in a mixture of DNA species with dynamic DNA structures (22). On the contrary, optical tweezers with the spatial resolution of 1 nm, force resolution of 0.1 pN, and temporal resolution of milliseconds (23) provide a much reliable in-situ setup for identifying interchangeable secondary and tertiary structures of DNA. After we analyzed unfolding pathways of structures formed in this region with and without PA-PDS conjugate, or its individual component (PA or PDS), we found different G-quadruplex structures in the hTERT 5–12 fragment can interconvert into each other. In particular, the PA moiety facilitates the formation of a complex G-quadruplex that contains a PA-recognizing loop whereas the PDS alone promotes the formation of tandem G-quadruplexes. Since the hTERT expression is modulated by particular GQ structures formed in this region (24), our results suggest that conjugates of a GQ-ligand and a dsDNA binder may serve as a new class of drugs that provide better synergistic specificity to target a promoter region involving both GQ and dsDNA. Polymerase stop assay and dual luciferase assay provided necessary insights on the effectiveness of the conjugate ligand PA-PDS over its standalone ligands PA or PDS.

Materials and methods

Materials

All the DNA oligonucleotides used for the experiments were purchased from IDT (Integrated DNA technologies, IA) and enzymes were purchased from NEB (New England Biolabs, England). Both the streptavidin-coated polystyrene beads (1.76 μm) and anti-digoxigenin antibody-coated polystyrene beads (2.32 μm) were obtained from Spherotech (Lake Forest, IL). All other chemicals and reagents were purchased from Sigma Aldrich or Fisher Scientific, unless otherwise stated, and were used without further purification. Bacterial plasmid for dual luciferase assay was obtained from Addgene.

Preparation of DNA constructs

All the DNA oligonucleotide sequences used in the study are listed in Supplementary Table S1. The general protocol for the preparation of DNA constructs is shown in Supplementary Figure S1 and respective agarose gel electrophoresis image in Supplementary Figure S2. The DNA of interest (hTERT 5–12) was flanked with 30-nt ssDNA sequence on 5′ end and 26-nt ssDNA sequence on 3′ end that had a sequence complementarity to hTERT 3 and hTERT 4 HF oligos respectively. This sequence was phosphorylated at 5′ end using T4 Polynucleotide Kinase and then annealed to hTERT 3 and phosphorylated hTERT 4 HF oligonucleotides. The annealing was carried out by heating at 95°C for 5 min and then cooled to room temperature in ∼2 h with a temperature ramping rate of 1°C/min. Finally, the annealed construct was ligated with 1558 bp and 2391 bp dsDNA handle by T4 DNA ligase at 16°C for 16 h. The 1558 bp handle was priorly labelled with biotin on its 5′ end by PCR, while 2391 bp handle was labelled with digoxigenin in its 3′ end by terminal transferase and dig-dUTP. The agarose gel image (Supplementary Figure S2) represents the successfully prepared construct.

Synthesis of PA and PA-PDS conjugate ligands

PA. A pyrrole-imidazole polyamide (PA) was synthesized, purified, and analyzed, as previously described (9). In brief, the PA chain was synthesized from a Fmoc-protected *N*-methylpyrrole-oxime resin using Fmoc-solid phase synthesis with a PSSM-8 computer-assisted operation system (Shimadzu) on a 0.02–0.04 mmol scale. The resulting resin was cleaved with *N*,*N*-dimethyl-1,3-propandiamine for 3 h at 45°C, and then the reaction mixture was directly poured into diethyl ether to be precipitated. The obtained precipitates were treated with 20% TFA in dichloromethane for 30 min at room temperature to deprotect the Boc group at the a-position of g-aminobutyric acid moiety and then purified by reverse-phase HPLC to give PA. Analytical HPLC: t_R = 12.6 minutes (0–75% MeCN/0.1% TFA over 30 minutes, detected at 254 nm). MALDI-TOF-MS *m/z* calcd for $C_{42}H_{55}N_{18}O_7^+$ $[M + H]^+$ 923.450 and found 923.604.

PA-PDS. The main chain of PA was built using an Fmoc-solid phase synthesis as mentioned above. On the resin, the Boc group at the a-position of g-aminobutyric acid moiety was deprotected with 20% TFA in dichloromethane for 30 minutes at room temperature, then three iterative reactions using {2-[2-(Fmoc-amino)ethoxy]ethoxy}acetic acid were performed to incorporate a linker motif. After the resin was cleaved with *N*,*N*-dimethyl-1,3-propandiamine for 3 hours at 45°C, the linker-containing PA was precipitated with diethyl ether. The subsequent coupling reactions of PA and azide-modified PDS were performed according to our previous literature (25). In brief, the precipitates were dissolved in dry DMF and DIEA. Dibenzocyclooctyne-*N*-hydroxysuccinimidyl ester was added to the mixture, then the reaction mixture was stirred for 3 h at room temperature. After the evaporation, azide-modified PDS was added to the solution of the crude compounds in DMSO, then stirred overnight at room temperature. The crude compounds were purified by reverse-phase HPLC to give PA-PDS. Analytical HPLC: t_R = 16.0 min (0–75% MeCN/0.1% TFA over 30 min, detected at 254 nm). MALDI-TOF-MS *m/z* calcd for $C_{110}H_{131}N_{32}O_{23}^+$ $[M + H]^+$ 2268.006 and found 2268.083.

Single molecule experiments

The instrument setup for optical tweezers used for the single molecule experiments has been reported elsewhere (26). To start single-molecule experiments, as-synthesized DNA constructs (see Supplementary Figure S1) with end labeled biotin and digoxigenin were incubated with streptavidin coated polystyrene beads (1.76 μm diameter) for 15 min to allow the DNA molecules to bind to the bead surface via the biotin-streptavidin linkage. In a three-channel microfluidic chamber, the streptavidin coated bead carrying DNA molecules (dissolved in 10 mM Tris and 100 mM KCl, pH 7.4) was injected into top channel while anti-Dig coated beads (2.32 μm diameter, dissolved in 10 mM Tris and 100 mM KCl, pH 7.4) were injected to bottom channel. These two channels were connected to middle reaction channel via capillary tubes (King Precision Glass, Inc., PO MC 7701, inner diameter 0.025 ± 0.010 mm). These two types of beads were separately trapped by two laser foci in the middle reaction channel. Two beads were then moved closer such that DNA molecule gets tethered between beads via anti-Dig/digoxigenin linkage and biotin/streptavidin linkage. Next, a force of loading rate ∼5.5 pN/s (at 10–30 pN range) was applied such that the DNA construct was unfolded during the extension. After reaching a specific force, the force was relaxed to zero at the same loading rate to allow the structure to refold before subsequent pulling. The single tether was confirmed by a single breakage event or plateau at ∼65 pN for the tethered DNA construct (27). All data were recorded in Labview™ (National Instruments, Austin, TX) and analyzed using Matlab™ and Igor™ programs. The rupture force was measured directly from the force–extension (*F*–*X*) curves, whereas the change in contour length (ΔL) was calculated from the two data points flanking the rupture event using the worm like chain (WLC) model given by Equation (1).

$$\frac{\Delta x}{\Delta L} = 1 - \frac{1}{2}\left(\frac{k_B T}{FP}\right)^{1/2} + \left(\frac{F}{S}\right) \quad (1)$$

where Δx is the change in end-to-end distance at the particular force F, k_B is the Boltzmann constant, T is absolute temperature, P is the persistent length (51.95 nm (28,29)), and S is the elastic stretch modulus (1226 pN (28,29)).

Polymerase stop assay

The DNA polymerase stop assay was performed according to previously established protocol (25). In brief, we synthesized a DNA template in which the hTERT 5–12 DNA (see Figure 1 for sequence) was placed upstream to a random DNA sequence (5′-TTAGCCAGCAAGACGTAGCCCAGCGCGTC-3′) capable of hybridizing to a 5′-Cy3 labelled primer (5′-Cy3-GACGCGCTGGGCTACGTC-3′). A reaction mixture containing the DNA template (2.5 pmol), BSA (1×), KCl (30 mM) and ligands (12.5 pmoles) was incubated in a phi29 DNA polymerase buffer (1×) at room temperature (25°C) for 30 min to form G-quadruplex–ligand complex. Primer extension was performed by adding 2 U of phi29 DNA polymerase enzyme along with 1 mM dNTPs at 30 °C for 1.5 h. Two separate reaction mixtures: one without phi29 DNA polymerase and the other without KCl were also prepared as control reactions. Finally, the enzymatic reaction was stopped by addition of 8 μl of alkaline loading buffer (Formamide 95% and 10 mM NaOH), heated at 95°C for 10 min, and cooled on ice for 5 min. The reaction mixture was then concentrated to ∼10 μl before loading into 16% denatured PAGE and run for 2 h at 65W. The gel image was recorded using Typhoon FLA 9500 (GE Healthcare, Cleveland, OH, USA) and quantified using ImageJ software (https://imagej.nih.gov/ij/). Dideoxy sequencing reactions were carried out with the same DNA template (2.5 pmol), dNTPs (1 mM) and ddNTPs (200 mM) to provide a sequencing ladder for assignment of the DNA polymerase arrest sites by adding 2.5U Taq DNA polymerase at 37°C for 45 min.

Dual luciferase assay

A dual luciferase assay was performed to evaluate the *in cellulo* efficacy of respective ligands (PA, PDS and PA-PDS conjugate) on hTERT 5–12 DNA using a simple gene expression system. For this assay, dual luciferase vector pC-KIT1 (Plasmid #118983, Addgene) was purchased and cloned with hTERT 5–12 DNA. First, pC-KIT1 vector was digested by the restriction enzymes NheI and BglII (NEB). Next, hTERT 5–12 duplex DNA was ligated into the pC-KIT1 vector by T4 DNA ligase (NEB). Finally, correct clones were established by digestion pattern with EcoRI-HF (NEB) in agarose gel electrophoresis, followed by confirmation from DNA sequencing (University of Maine, Orono).

For dual luciferase assay, HEK293T cells (ATCC CRL-3216™) were maintained in DMEM supplemented with 10% FBS (Gibco) at 37 °C and 5% CO_2. The cultured cells were then seeded at a density of 4 × 10^4 cells/well in a 96-well plate (Corning® 96-well Clear Flat Bottom-3598) and co-transfected with hTERT cloned vector (200 ng/well) along with 5 μM ligands (PA, PDS, or PA-PDS), using the GenJet™ Plus transfection reagent (SignaGen Laboratories). After 24 h of transfection, the level of expression of the dual luciferase reporter genes was measured following the manufacturer's protocol of Pierce™ Renilla-Firefly Luciferase Dual Assay Kit (ThermoFisher Scientific-16185) in a bioluminescence detector (FLx800™ Fluorescence Microplate Reader, BioTek Instruments).

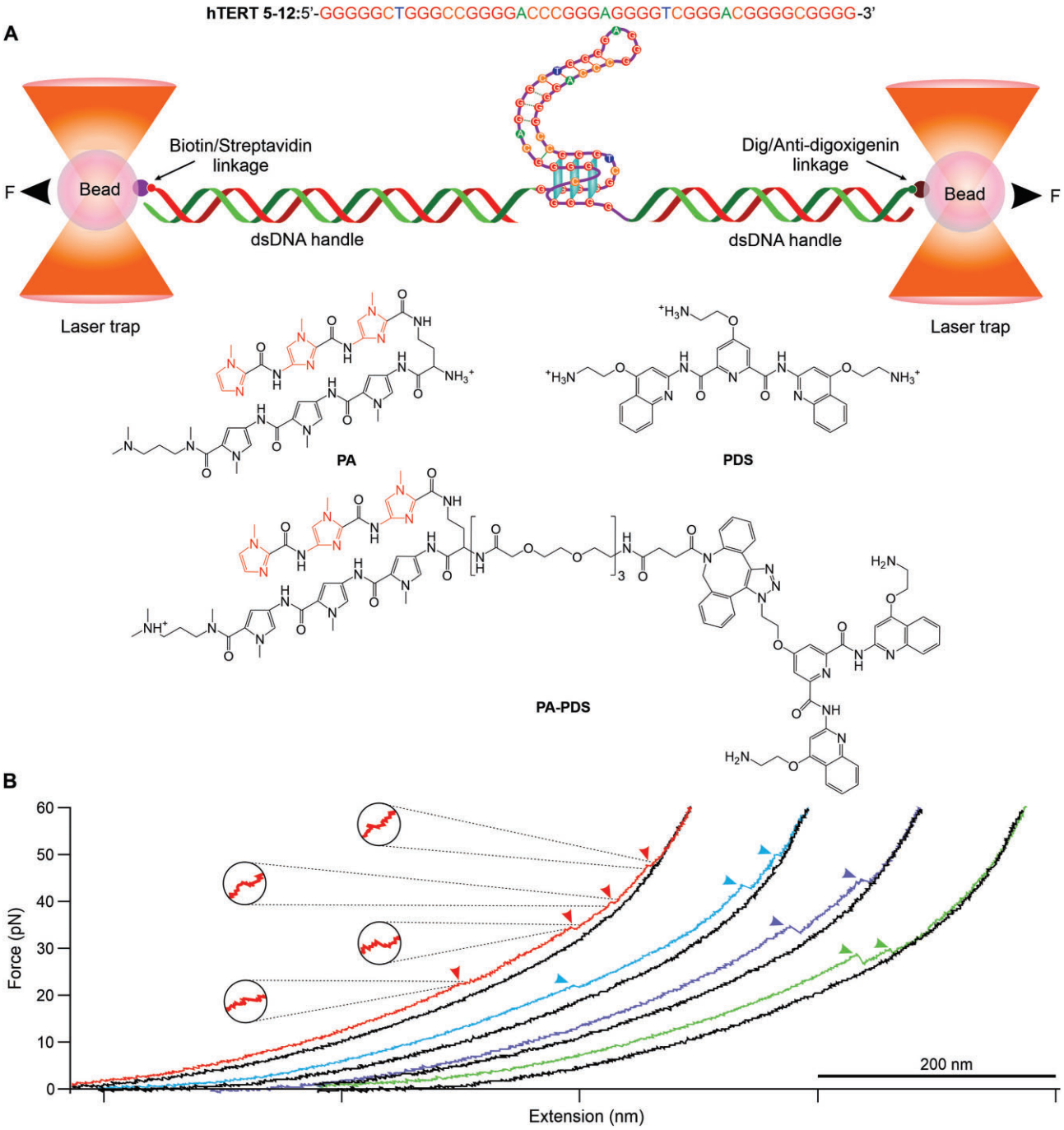

Figure 1. (**A**) Optical-tweezers setup to investigate G-quadruplex folding patterns in presence of ligands PA, PDS, and PA-PDS. The hTERT 5–12 containing DNA fragment (sequence shown on the top) was tethered between two dsDNA handles, which are separately labelled with biotin and digoxigenin on their ends. Biotin links to the streptavidin-coated beads and digoxigenin is tethered to the digoxigenin-antibody-coated bead. Both beads are separately trapped by two laser foci. (**B**) Representative stretching (colored) and relaxing (black) F-X curves showing four, three, and two unfolding features depicted by arrowheads in different molecules without any ligand in a 10 mM Tris buffer (pH 7.4) with 100 mM KCl at 23 °C.

Results and discussion

Preparation of ligands and DNA constructs.

To investigate the G-quadruplex structures formed in the hTERT promoter region (from the position −90 to −46, designated as hTERT 5−12), a DNA fragment, 5′-GGG GGC TGG GCC GGG GAC CCG GGA GGG GTC GGG ACG GGG CGG GG-3′, was sandwiched between two dsDNA handles with 1558- and 2391-bp in length (see Supplementary Figures S1 and S2 for details). The whole construct was then tethered between two beads: one bead coated with streptavidin that could complex with the biotin-labeled 1558 bp DNA handle while the other bead coated with anti-digoxigenin would form a linkage with the digoxigenin labelled 2391 bp DNA handle (Figure 1A). These two beads were then trapped using two laser foci and pulled apart to record the force in the DNA tether and the change in extension between two optically trapped beads in a laser-tweezers instrument.

From previous studies (17,30), it was found that the folded structure in the hTERT 5–12 contains a G-quadruplex with a long hairpin loop. However, recent study provides another insight indicating that the core promoter of hTERT folds into tandem G-quadruplexes (19). To probe the exact folding mechanism of hTERT, we designed three ligands that bind to specific structural elements. First, a PA (13) was designed to specifically bind to the hairpin stem. Next, a PDS (15) was used to bind to a terminal G-quartet in a G-quadruplex structure. Lastly, a conjugate of PA and PDS was prepared to bind the whole hairpin-GQ structure. Individual structures of each ligand are shown in the lower panel of Figure 1A.

PA was synthesized using an Fmoc solid-phase synthesis, as previously described (9). For the synthesis of the PA-PDS conjugate, three consecutive linkers were iteratively incorporated into PA on a resin. After the cleavage from the resin, the resultant linker-containing PA compounds were modified with an azadibenzocyclooctyne unit, which was used for the subsequent coupling with azide-modified PDS via strain-promoted azide–alkyne cycloaddition (31). The final products of PA and PA-PDS were purified by HPLC and analyzed by mass spectrometry (see Supplementary Figure S3 and S4).

Unfolding of hTERT 5–12 structures follows either sequential or cooperative pathways

We investigated the unfolding patterns of structures formed in the hTERT 5–12 fragment using the optical tweezers shown in Figure 1A. During the unfolding experiment performed in a 10 mM Tris (pH 7.4) buffer with 100 mM KCl at 23 °C, the force was increased with a load rate of 5.5 pN/s (in the range of 10–30 pN). The force-extension (F-X) curves obtained (Figure 1B) showed multiple unfolding features. When we repeated experiment in the same buffer with 100 mM LiCl, unfolding features disappeared, which was consistent with previous finding (17) that G-quadruplexes have been formed in this fragment since Li^+ is known not to facilitate GQ formation (32,33). As each *F–X* curve contains a distinct pattern of these unfolding features, it is likely that different unfolding pathways exist. To interrogate these unfolding pathways, we analyzed the *F–X* curves obtained from fully folded structures, which were revealed from the maximum change-in-contour-length (ΔL) value obtained during mechanical unfolding processes (ΔL = 15.8 nm for fully folded to fully unfolded states, see Supplementary Information for details). Since multiple featured traces with as small as 3 nm could be formed and not well differentiated in the regular *F–X* curves, we transposed those traces into ΔL versus *F* plots (34) for a better resolution. To make a fair comparison on the unfolding size (ΔL) of each intermediate without interference from the baseline drift in the force ramping procedure, we converted *F–X* curves to ΔL versus *F* plots (Figure 2, see Supplementary Information for details (17)). These ΔL versus *F* plots allowed us to identify several intermediates involved in each of the unfolding pathways (Figure 2). Each step in Figure 2 corresponds to a feature obtained in traces such as those shown in Figure 1B. In the unfolding of the hairpin-GQ structure, these intermediates may involve partial unfolding of the G-quadruplex (stabilized by a G-duplex (18)), the intact hairpin loop (25-nt), and the 15-nt hairpin in the loop (17)). In the unfolding of the two tandem GQs, three intermediates may consist of a GQ with a G-triplex (35), a GQ and a G-triplex. Close inspection on these ΔL versus *F* plots revealed that unfolding's of hTERT GQ structures follow either cooperative (brown) or sequential (other colors) pathways, which is consistent with previous reports (17).

When we compared the pattern of unfolding pathways for the structures formed in the hTERT 5–12 fragment without (control) and with 500 nM PA, PDS or PA-PDS, we found that the unfolding patterns in presence of PDS are more similar to the control whereas those in presence of PA or PA-PDS deviate more from the control. We used 500 nM PA in our study, which is much higher than the K_d (∼35 nM) of the binding between a similar PA and a 6-bp DNA sequence (25), ensuring a complete binding of PA to the specific dsDNA sequence. When we performed force ramping experiments on a random DNA hairpin flanked by the same dsDNA handles (see Supplementary Figure S5), we did not observe much noise in the force extension curves. This observation was in contrast to the notable noise manifested at higher PA concentration (5 μM), suggesting negligible PA binding to the dsDNA handles at 500 nM PA. The percentage abundance analysis of pathways in Figure 2 revealed that seven out of eight pathways (red, cyan, green, purple, grey, orange and dark blue) followed the same ranking order between the control and PDS, whereas the ranking orders were significantly deviated when the control was compared to PA or PA-PDS. Hierarchical cluster analysis (HCA) (36) confirmed the similarity in the unfolding pathway patterns: PDS and the control shared similar unfolding pathways whereas PA deviated from the unfolding patterns of PDS (Figure 3, see Supplementary Information for detailed statistical analysis of HCA). Finally, PA-PDS showed an unfolding pathway pattern that is different from either PA or PDS.

In presence of 500 nM PA, since the polyamide is expected to bind to the duplex hairpin stem formed in one of the loops in the GQ-hairpin structure (25) (Figure 4A), we argued that such a structure should be facilitated when PA binds. On the other hand, since PDS is a GQ binder, it will promote the formation of maximal number of GQs. We therefore reasoned that two tandem GQs are more likely formed in presence of PDS (Figure 4A). Given that the control shares a similar unfolding pattern as the PDS (see HCA dendrogram in Figure 3), the tandemly formed GQs likely exist when there is no ligand. However, as PA-PDS contains both PA and PDS components, the unfolding pathway pattern might show a mixed unfolding patterns corresponding to individual ligands.

Further evidence for the assignment of unfolding pathways in presence of different ligands comes from unfolding experiments using truncated DNA sequences. Three truncated hTERT 5–12 DNA fragments were used (Figure 4B), which include a 15-nt short hairpin (5′GACCCGGGAGGGGTC), a 24-nt 5′ G-quadruplex (5′GGGGGCTGGGCCGGGGACCCGGGA), and a 20-nt 3′ G-quadruplex (5′GGGGTCGGGACGGGGCGGGG). CD spectra showed two distinct peaks at ∼260 nm and ∼290 nm, characteristic features of G-quadruplexes (see Supplementary Figure S6) (37). After mechanical unfolding experiments, the rupture forces for each of those truncated structures without (control) and with ligands (500 nM each of PA, PDS or PA-PDS in Tris-KCl buffer with 100 mM KCl at pH 7.4 at 23 °C) were recorded and presented in force histograms (Figure 4B). The change-in-contour-length (ΔL) histograms are presented in Supplementary Figure S7.

In presence of the PDS, the force histogram of the 15-nt short hairpin showed one peak with an average force of 16 pN, which was similar to that of control (∼15 pN) without

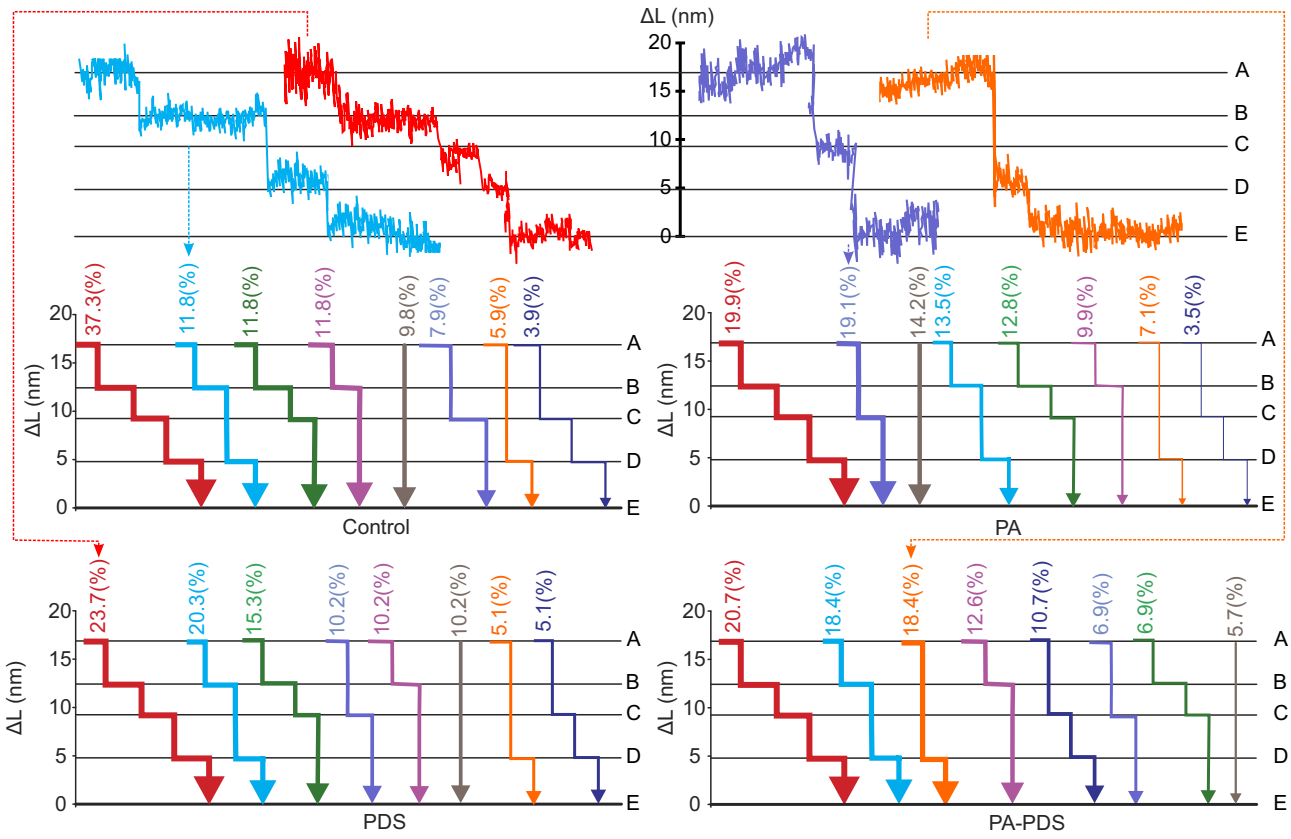

Figure 2. Representative traces of unfolding pathways (upper panel). The middle and lower panels represent percentage probability of different pathways without and with ligands.

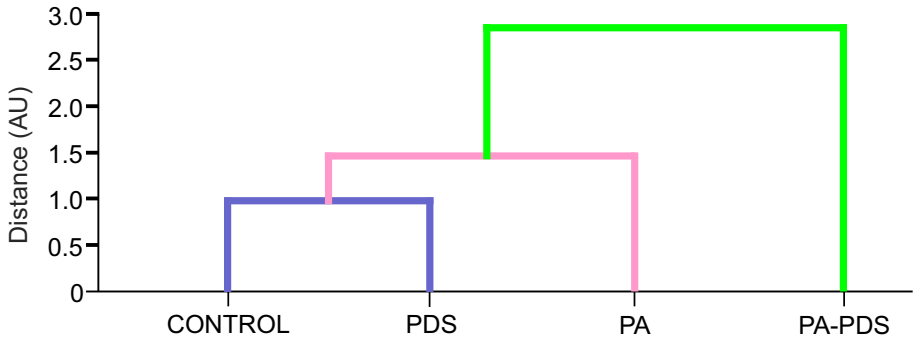

Figure 3. Dendrogram obtained from Hierarchical Cluster Analysis shows the similarity among unfolding patterns of hTERT 5–12 without and with PA, PDS or PA-PDS ligands.

ligand. However, a higher force population (∼41 pN) was obtained when the structure was unfolded in presence of PA. This population disappeared when PDS was present. All these results suggest that the 15-nt hairpin contains the binding site for PA but not for PDS. A similar two-peak (∼16 and 39 pN) force histogram was obtained with PA-PDS, confirming the binding of the ligand via the PA moiety. High-force population in PA and PA-PDS strongly suggested that the binding site of PA is at the neck region of the hairpin where the transition state is located for hairpin unfolding (38).

Next, we evaluated the ligand binding on the 5′- (24-nt) or 3′- (20-nt) end GQ forming fragment (Figure 4B). We found that higher force populations were present when there was 500 nM each of PDS (∼38 pN) or PA-PDS (∼40 pN) in buffer. In contrast, PA and the control shared similar unfolding force histograms without high-force populations. This implied that PDS indeed binds to either 5′- or 3′- end GQ in the hTERT 5–12 region. From these sets of experiments, we confirmed that specific binding sites in truncated hTERT sequences may associate with the corresponding DNA binding ligands to influence the folding of different structures.

Unfolding pathways of hTERT 5–12 structures in the presence of different ligands.

With the structures clarified in presence of ligands, we proceeded to investigate the effects of ligands on each unfolding step. Based on the above results, we formulated that the

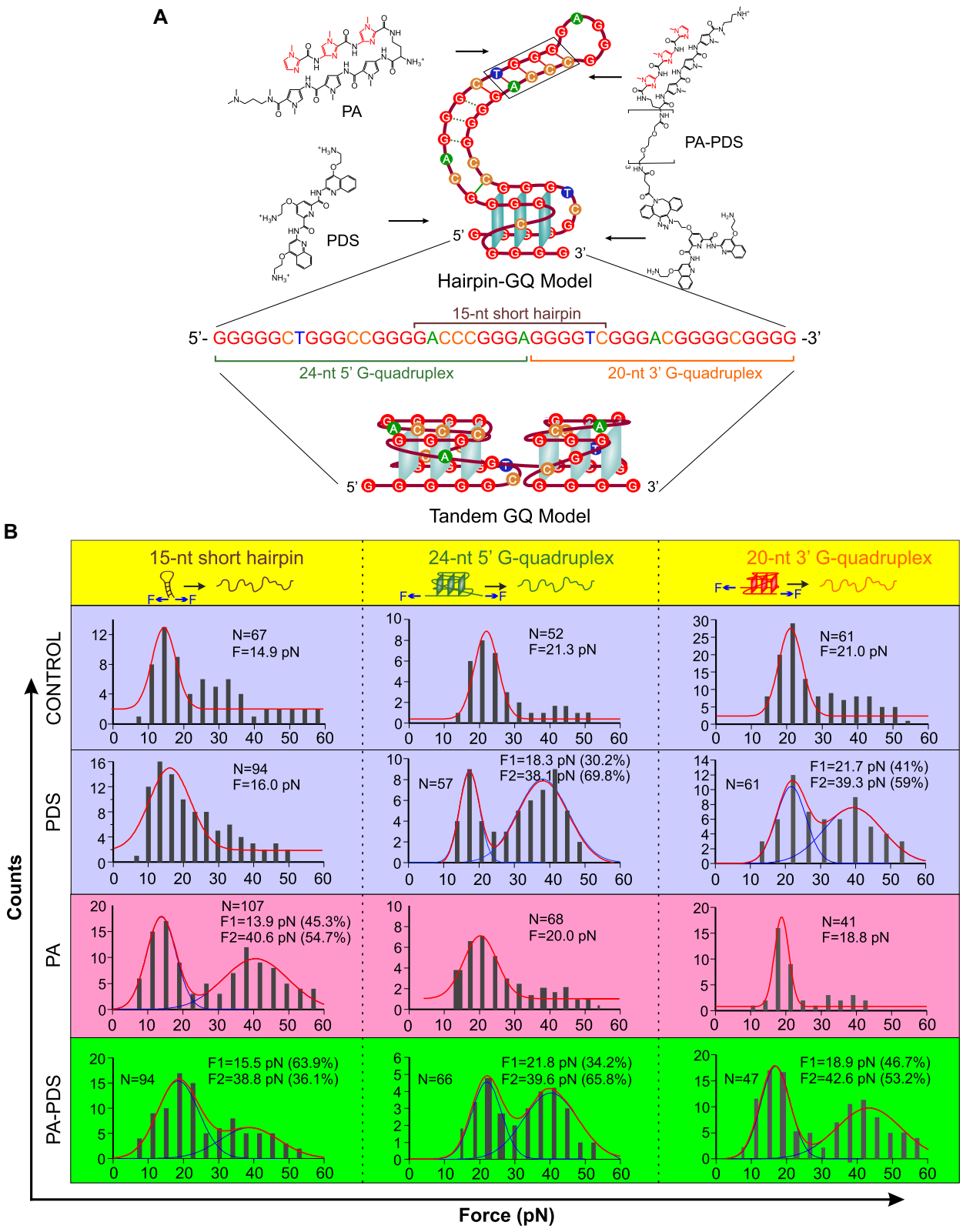

Figure 4. (**A**) Two hTERT structure models marked with binding sites for individual ligands. Truncated sequences (15-nt short hairpin, 24-nt 5′ G-quadruplex, and 20-nt 3′ G-quadruplex) are denoted along the hTERT 5–12 sequence. (**B**) Unfolding force histograms for each truncated structure without and with ligands. Experiments were performed in presence of 500 nM of PA, PDS, or PA-PDS in a 10 mM Tris–100 mM KCl buffer at pH 7.4 at 23 °C. *F* represents force. *N* depicts the number of features.

unfolding of hTERT 5–12 structures follows four stepwise unfolding transitions via three intermediates. However, specific unfolding transitions could be from different folded hTERT 5–12 structures dependent on ligands. For example, unfolding pattern can be represented by Pathway 1 starting from the two tandem G-quadruplexes (Figure 5). Depending upon ligands, this Pathway 1 can be further divided into Branch 1 or Branch 2 depicted in Figure 5 top and bottom panels, respectively. Branch 1 consists of 3 intermediates: an intact G-quadruplex with G-triplex, two G-triplexes, and a G-triplex with a fully unfolded G-quadruplex. On the other hand, Branch 2 has another set of intermediates: an intact G-quadruplex with G-triplex, an intact G-quadruplex with a fully unfolded G-quadruplex, and a G-triplex with a fully unfolded G-quadruplex. Although these are likely pathways, we do not rule out the presence of other possible models. In another example, in the unfolding pathway 2 (Figure 6), a fully folded 42-nt structure is unfolded en route to the intermediates of a 32-nt structure (a 25-nt hairpin with a G-triplex), a 25-nt hairpin structure, and a 15-nt hairpin structure.

During each sequential mechanical unfolding step with and without ligands, we obtained unfolding force histograms (Figures 5&6). Overall, as the unfolding progresses from steps I to IV, there is an increment in the magnitude of the unfolding force due to the sequential unfolding nature. In the control experiment without any ligands (Figure 5), we observed a single force population concentrated at ∼21, 27, 37 and 51 pN for the transitions I, II, III and IV respectively. However, the unfolding force patterns altered in the presence of PDS. Since the PDS concentration used for the experiment (500 nM) was close to its K_d (39), we expect only one of the G-quadruplexes to be bound with the PDS ligand. In transition I, PDS showed a low force population centered at ∼19 pN, which is similar to that of the control (i.e. free G-quadruplex, ∼21 pN). The same transition also showed a high force population of 44 pN, likely due to binding of the PDS ligand to one of the G-quadruplex structures, increasing the mechanical stability. The transition II had a low-force unfolding population (centered at ∼20 pN) corresponding to a free G-Quadruplex without any bound PDS and a high-force population (∼37 pN) that may be ascribed to the unfolding of a PDS-bound G-triplex. In the transition III, the low-force population of ∼27 pN may be due to partial unfolding of a ligand-free G-Quadruplex while the high-force population of ∼37 pN could come from partial unfolding of the PDS bound G-Quadruplex. Finally, the transition IV revealed a force population centered at ∼53 pN, which can be ascribed to the transition to fully unfold structures. As this transition follows previous steps, it has the highest follow-through force. This feature prevents us from distinguishing PDS bound and unbound G-Quadruplexes by comparing the magnitude of the unfolding force only.

In presence of 500 nM PA, we obtained rather different histograms (Figure 6, upper panel) than that with PDS (Figure 5), suggesting that binding of the ligand may result in different folding patterns of hTERT 5–12 structures, which is consistent with what found in HCA in Figure 4. Here, we observed single force population (∼22 pN) in the transition I, which may correspond to the partial unfolding of G-Quadruplex to G-triplex. In the transition II, the G-triplex was unfolded, giving rise to a 38-nt hairpin with the unfolding force centered at ∼35 pN. The subsequent transition III showed the partial unfolding of the hairpin with force peak at ∼37 pN. Finally, the PA bound terminal hairpin was fully unfolded in transition IV with an unfolding force at ∼52 pN. Although PA has a binding site at the terminal end of the hairpin as shown in the pathway 1 in Figure 5, the unfolding event corresponding to that binding resulted in a force much higher than expected due to the tension accumulated in the template during the preceding transitions I–III (i.e. the follow-through force). Therefore, no distinction in the unfolding force of the transition IV can be observed among PA-bound and free hairpins.

Finally, force histograms were constructed for the unfolding of the hTERT 5–12 fragment in presence of 500 nM PA-PDS (Figure 6, lower panel). Here, the transition I gave a low-force population (∼20 pN) that is attributed to the unfolding of ligand free structures and a high-force population (∼41 pN) that is ascribed to the unfolding of a ligand bound hTERT 5–12 structure. The ∼30% high-force population in PA-PDS indicates that the ligand binds more strongly than the PDS (∼14% high-force population), likely due to the cooperative binding modes between PDS and PA. The transition II also contained two populations of ∼23 and ∼38 pN. The 38 pN population could be due to the PA-PDS binding to the G-quadruplex via the PDS moiety. Likewise, in the two unfolding forces observed the transition III (∼24 and ∼41 pN), the high force population could be ascribed to the PDS binding of the G-quadruplex in the structure. Finally, the transition IV contained the full unfolding of the structure (∼49 pN). The transition patterns observed during unfolding of the hTERT structures indicated that in presence of PA-PDS, the hTERT 5–12 sequence can adopt either of those two folding structures and the pathways can be a combination of both Pathways 1 and 2. All the change-in-contour-length (ΔL) histograms in presence and absence of ligands are presented in Supplementary Figure S8. The theoretical change-in-contour-lengths are enlisted in Supplementary Table S2.

One of the notable things is the difference in the unfolding behavior between truncated sequences (Figure 4) which is a single step unfolding and the hTERT 5–12 sequence (Figures 5 and 6) which is multi-step unfolding. Such a significant multi-step unfolding in hTERT 5–12 sequence can be accredited to the interaction of various intermediates, such as G-triplexes, to the G-rich sequences in the rest of the longer hTERT 5–12 fragment, which may stabilize these intermediates (40).

Polymerase stop assay exhibits synergistic binding of PA-PDS onto hTERT 5-12 structures.

To demonstrate an increased specificity of the conjugated ligand PA-PDS, we next performed the polymerase stop assays. We first designed a DNA sequence containing a primer binding site downstream to the hTERT 5–12 sequence (Figure 7A). Next, we annealed a primer DNA modified with 5′-Cy3 such that the highly processive phi29 DNA polymerase extended the primer against the hTERT 5–12 template strand when dNTPs were provided. The extension stoppage patterns were confirmed without and with 30 mM KCl (Figure 7B; lanes 2 and 3). With KCl, GQ formed in the template, which could pause the primer extension by the polymerase (25). The resultant pause bands matched with this GQ formation. The replication stop bands in presence of PDS and PA (Lanes 4 and 5, respectively) showed a significant difference, which signified different binding modes of these ligands. PDS enriched pause

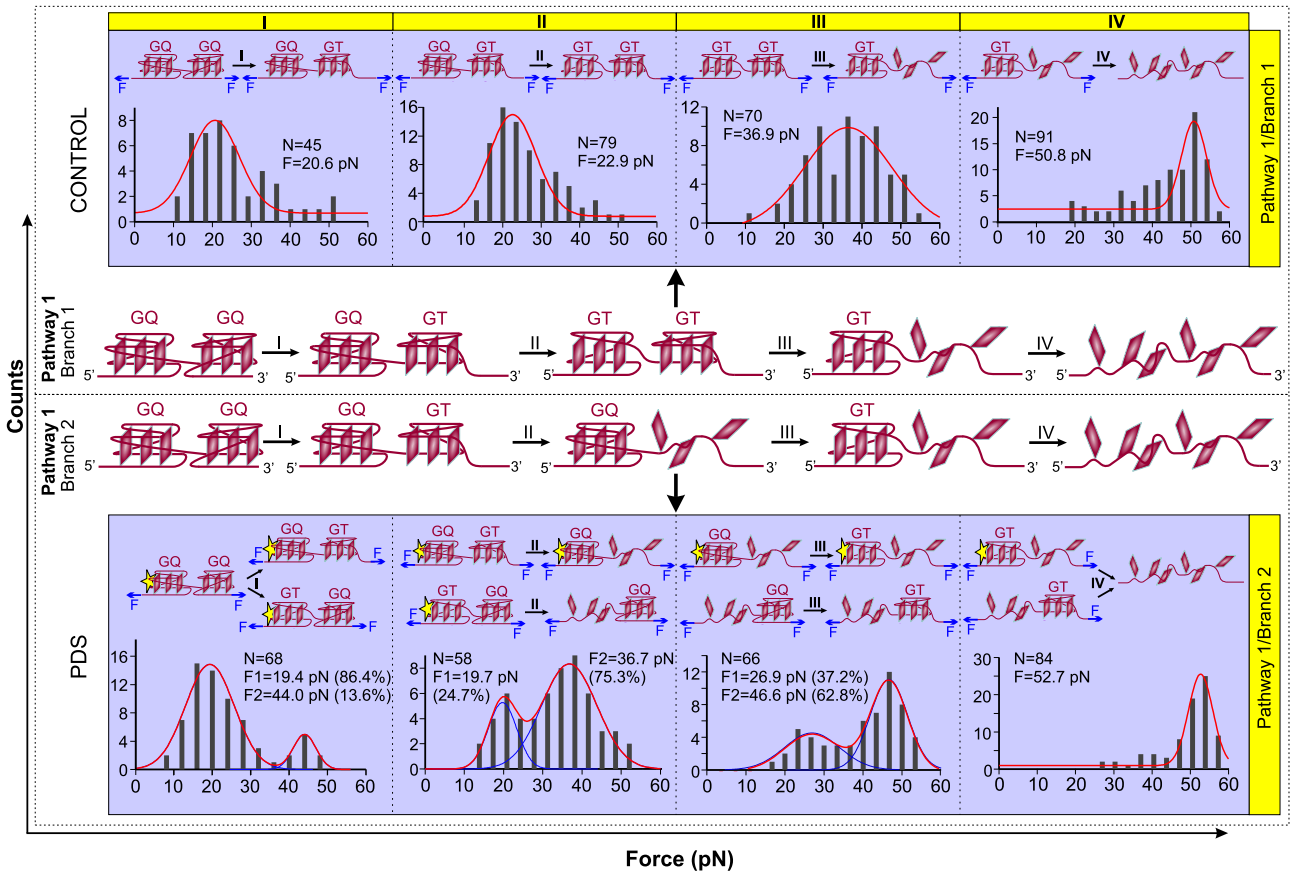

Figure 5. Unfolding force histograms recorded during the sequential unfolding of the hTERT 5–12 fragment without (control) and with 500 nM PDS in a Tris–KCl buffer (pH 7.4) at 23 °C. Each unfolding branch of the Pathway 1 is depicted by schematics below each panel. GQ and GT depict G-quadruplex and G-triplex, respectively. *F* represents force while yellow star represents PDS ligand. *N* depicts the number of features.

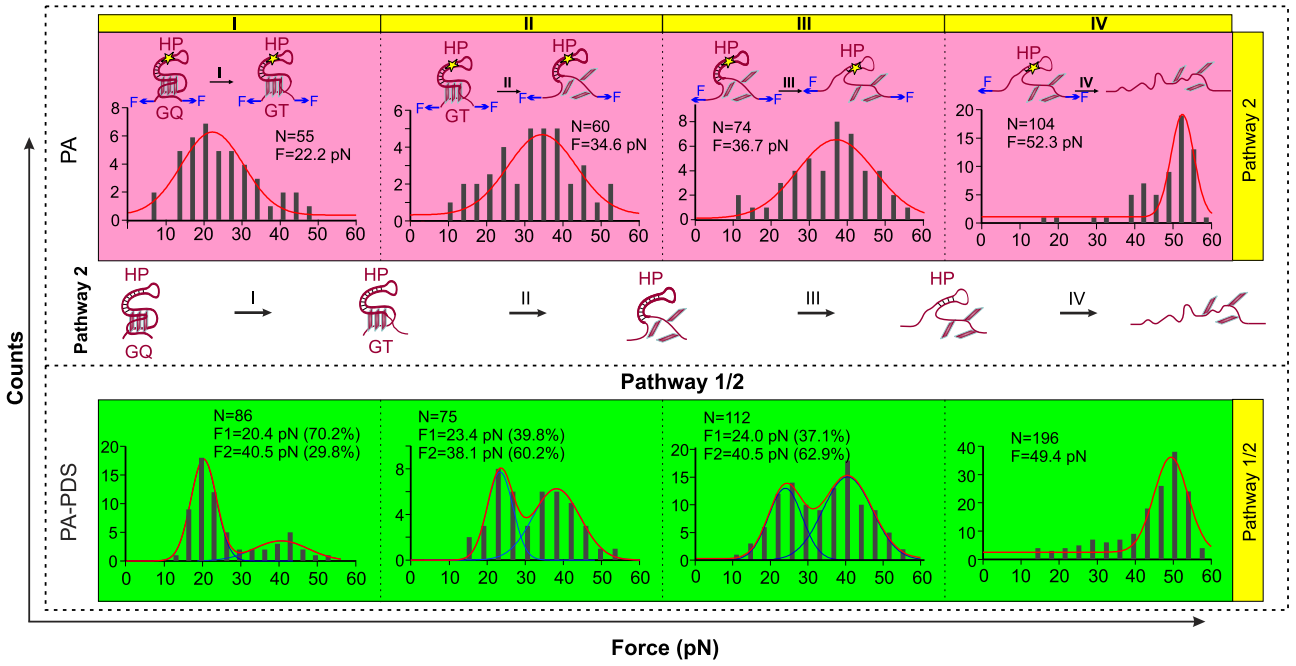

Figure 6. Unfolding force histograms recorded during the sequential unfolding of the hTERT 5–12 fragment with 500 nM PA or PA-PDS in a Tris–KCl buffer (pH 7.4) at 23 °C. The schematics of the unfolding Pathway 2 of the hTERT 5–12 structures is shown below the top panel. Unfolding pathway in presence of PA-PDS is a combination of Pathway 1 (shown in Figure 5) and Pathway 2. GQ, GT and HP depict G-quadruplex, G-triplex and Hairpin, respectively. *F* represents force while yellow star represents PA ligand. *N* represents the number of features.

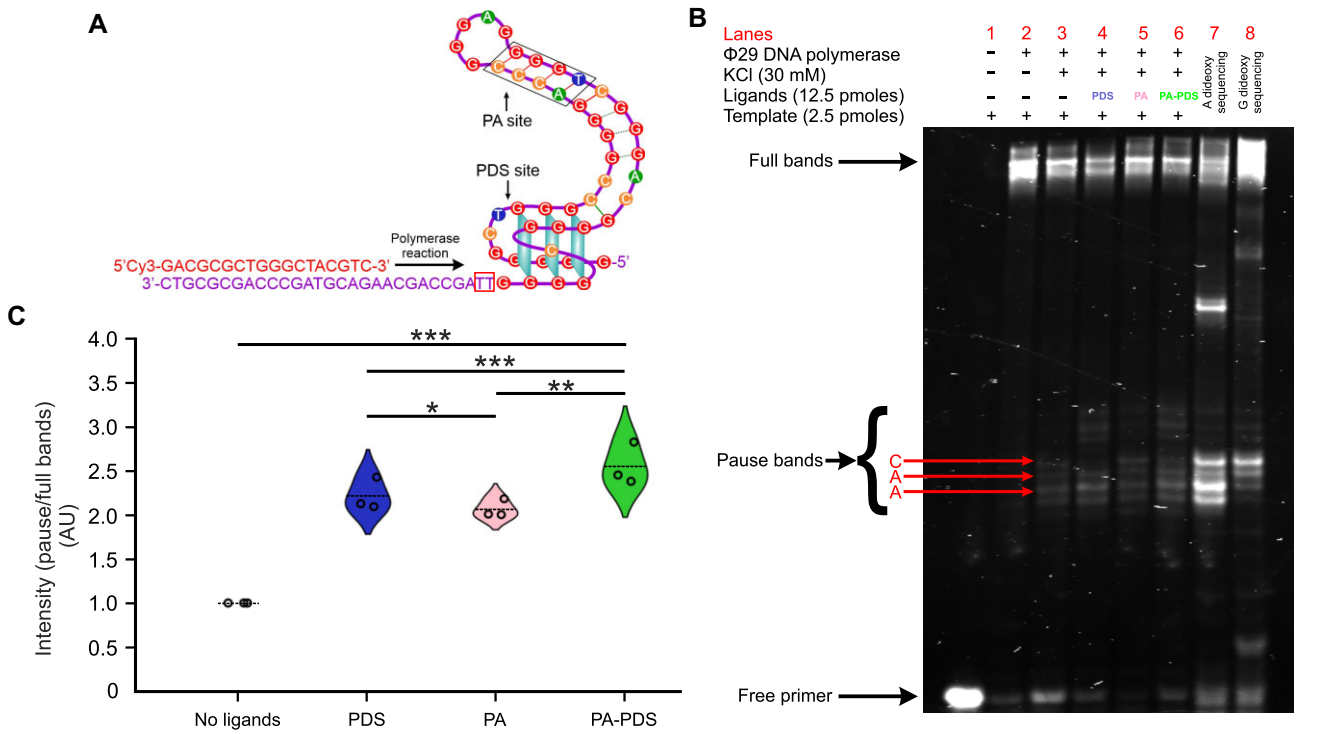

Figure 7. Polymerase stop assay with and without ligands. (**A**) Schematic design of the hTERT 5–12 templating strand and Cy3-labeled primer. The 5′-Cy3 labeled primer (shown in red) was annealed at the 3′ end (shown in purple) of the hTERT 5–12 sequence. (**B**) Denaturing PAGE gel analysis of the products from the polymerase stop assay under different conditions labeled on top. Lanes 7 and 8 represent products from A and G dideoxy sequencing, respectively (see Supplementary Figure S9 for detailed analyses). Black arrows on the left indicate positions of the full bands, pause bands and free primer, while red arrows indicate specific positions of the extended product in the pause bands. (**C**) Violin plots representing the intensity ratio of the paused to full bands in absence and presence of ligands (lanes 3 to 6 from Figure 7B). Single, double, and triple asterisks indicate significant differences at $P < 0.1$ (>90% CL), $P < 0.05$ (>95% CL) and $P < 0.01$ (>99% CL) by paired *t*-test, respectively.

bands at the AA site (marked with the red arrows in Figure 7B; see the complementary TT site in the template strand marked by the red box in Figure 7A) in front of the G-quartet. Such an observation is consistent with the binding of the PDS to the external G-quartet facing the AA site. In presence of PA, the pause bands were reduced (Figure 7B, lane 5), reflecting its decreased capability to promote GQ formation. However, since it is designed to bind the hairpin formed in one of the GQ loops, it still promoted the GQ formation as the hairpin served as the nucleation for the hTERT GQ formation (17). When PA-PDS bound to the hTERT fragment (lane 6), it brought a synergistic effect of both PDS and PA, leading to strongest pause bands.

Analyses on the paused to full band intensity ratios confirmed this observation (Figure 7C). The PA-PDS indeed showed an increased ratio compared to standalone PDS or PA. A two-tailed paired t-test results indicated significant differences at $P < 0.01$ (>99% confidence level (CL) and $P < 0.05$ (>95% CL), respectively, between PA-PDS and PDS, and between PA-PDS and PA. These results confirm the increased specificity of the conjugate ligand PA-PDS to recognize GQ structures formed in the hTERT 5–12 fragment.

PA-PDS presents high efficiency in driving gene expression in cells.

Inspired by the increased specificity of PA-PDS from the results of polymerase stop assay, we next questioned whether the conjugate ligand PA-PDS would demonstrate higher perturbation of gene expression in cells compared to its standalone counterparts. To evaluate the effects of the ligands (PA, PDS and PA-PDS) on the protein expression controlled by the hTERT 5–12 DNA promoter, we performed a dual luciferase assay by cloning the hTERT 5–12 sequence into the promoter region of the *Renilla* gene while keeping the HSV TK promoter unchanged which controlled the expression of *Firefly* (Figure 8A). As these two genes express two luciferases that separately convert substrates to products with different colors, we can quantify the effect of each ligand by measuring the luminescence of the product catalyzed by Renilla luciferase over that by Firefly luciferase. After preforming at least three biological replicates in HEK293T cells transfected with the cloned plasmid (Figure 8A), we normalized the luminescence ratio of each ligand against that of the control where HEK293T cells contained plasmid alone without any ligands. Compared to the control, Renilla luciferase activity was significantly reduced in cells incubated with each ligand (Figure 8B). Notably, its activity decreased more in cells transfected with PA-PDS than those transfected with PA ($P < 0.001$, two-tailed paired t-test, CL > 99.9%) or PDS ($P < 0.01$, CL > 99%) alone. Given the fact that small molecules like PDS are much easier to enter cells compared to bigger molecules such as PA or PA-PDS (41,42) (the cell bioavailability difference between PDS-like small molecules and PA is at least 10 times, with even more for PA-PDS), these data unequivocally established the more pronounced effect of PA-PDS over PDS or PA in the gene expression via interaction with hTERT5-12 G-quadruplex structures inside cells.

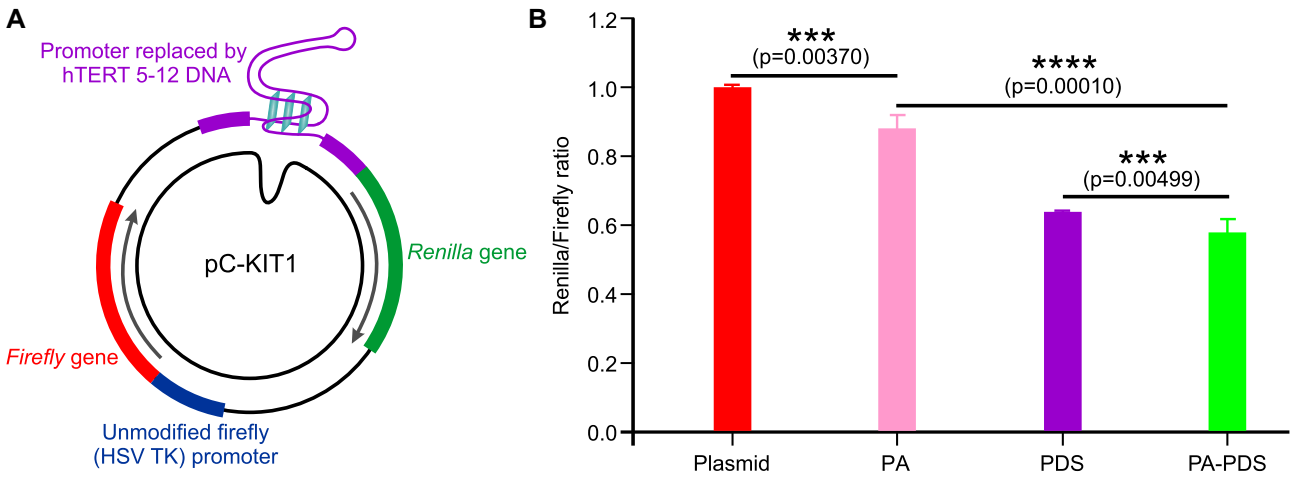

Figure 8. (**A**) A dual luciferase plasmid system based on the pC-KIT1 (Addgene) was constructed with hTERT 5–12 DNA inserted in the promoter region that controlled *Renilla* gene expression while the promoter (HSV TK) was unmodified that controlled *Firefly* gene expression. Arrows depict the direction of gene expression. (**B**) Ratiometric evaluation of *Renilla* to *Firefly* gene expression for the HEK293T cells transfected by the plasmid shown in (A) with 5 μM each of PA, PDS or PA-PDS ligand. The ratio of Renilla versus Firefly luciferase activity was normalized with respect to that of the plasmid alone. Three and four asterisks indicate significant differences at $P < 0.01$ (>99% CL) and $P < 0.001$ (>99.9% CL) by paired t-test, respectively. Error bars on graphs represent standard error of mean (SEM). Numbers of independent experimental repeats are 5, 5 and 9 for PA, PDS and PA-PDS, respectively.

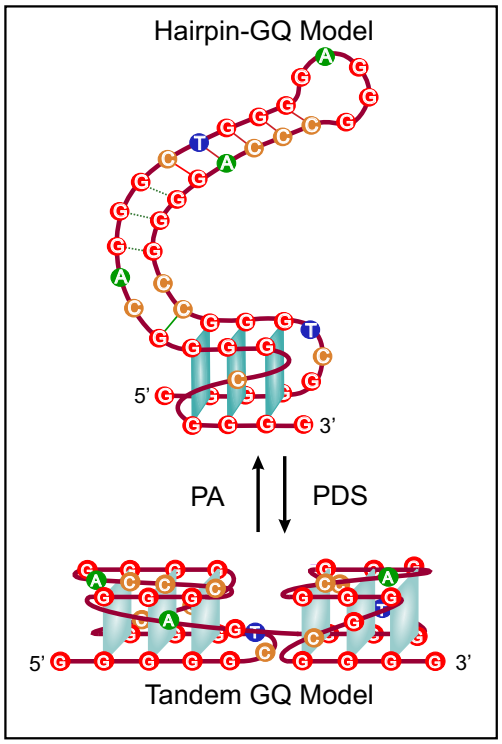

Figure 9. Schematics of two possible structures formed in the hTERT 5–12 sequence in presence of different ligands.

Conclusion

In summary, we designed a small molecule conjugate, PA-PDS, to target hTERT 5–12 promoter region by combining the duplex DNA binding domain (PA) and the G-quadruplex binding domain (PDS). Based on the unfolding force events obtained in an optical-tweezers setup, we found the folding patterns in the hTERT 5–12 fragment were rather dynamic. The sequence folds into the hairpin-GQ structure in presence of PA, whereas in presence of PDS, the DNA fragment forms two tandem GQs (Figure 9). This study provides new insights on different folded structures present in the hTERT 5–12 promoter region. The dynamic property can be used to design small-molecule ligands for specific targeting. Results from polymerase stop assay and dual luciferase assay demonstrated that a conjugate ligand PA-PDS has higher efficiency compared to its counterpart ligand of PA or PDS. Such a synergistic binding of conjugate ligand opens a broad direction for the development of small molecule conjugates for specific binding of G-quadruplex in a duplex DNA context.

Data availability

Any additional information required to analyze the data reported in this paper is available from the lead contact upon request.

Supplementary data

Supplementary Data are available at NAR Online.

Acknowledgements

D.K. thanks Mao group members for very helpful discussions. D.K. also thanks Mohammad Akter Hossain for the data collection.

Author contributions: H.M. conceptualized and supervised the project. D.K., L.L. and S.M. performed experiments on optical tweezers. S.A., Y.K., K.H., T.B. and H.S. synthesized the ligands. D.K. and G.S. performed dual luciferase assay. D.K., Y.K., H.S. and H.M. co-wrote the manuscript.

Funding

National Institute of Health [R01 CA236350 to H.M. and H.S.]; National Institute of Health [R01 CA252827 to H.M.]; National Science Foundation [CBET1904921 to H.M.]; Lundbeck Foundation [grant number R346-2020-1890 to H.M.]; Japan Society for the Promotion of Science

KAKENHI [20H05936 and 21H04705 to H.S.]. Funding for open access charge: NIH [R01 CA236350]. This publication was made possible in part by support from the Kent State University Open Access Publishing Fund.

Conflict of interest statement

None declared.

References

1. Henderson,E., Hardin,C.C., Walk,S.K., Tinoco,I. Jr and Blackburn,E.H. (1987) Telomeric DNA oligonucleotides form novel intramolecular structures containing guanine·guanine base pairs. *Cell*, **51**, 899–908.
2. Catasti,P., Chen,X., Moyzis,R.K., Bradbury,E.M. and Gupta,G. (1996) Structure-function correlations of the insulin-linked polymorphic region. *J. Mol. Biol.*, **264**, 534–545.
3. Simonsson,T., Pecinka,P. and Kubista,M. (1998) DNA tetraplex formation in the control region of c-myc. *Nucleic Acids Res.*, **26**, 1167–1172.
4. Huppert,J.L. and Balasubramanian,S. (2007) G-quadruplexes in promoters throughout the human genome. *Nucleic Acids Res.*, **35**, 406–413.
5. Kim,N.W., Piatyszek,M.A., Prowse,K.R., Harley,C.B., West,M.D., Peter,L.C.H., Coviello,G.M., Wright,W.E., Weinrich,S.L. and Shay,J.W. (1994) Specific association of human telomerase activity with immortal cells and cancer. *Science*, **266**, 2011–2015.
6. Raptis,S. and Bapat,B. (2006) In: *Cancer: Cell Structures, Carcinogens and Genomic Instability*. Birkhäuser Basel, Basel, pp. 303–320.
7. Shu,H., Zhang,R., Xiao,K., Yang,J. and Sun,X. (2022) G-quadruplex-binding proteins: promising targets for drug design. *Biomolecules*, **12**, 648.
8. Cadoni,E., De Paepe,L., Manicardi,A. and Madder,A. (2021) Beyond small molecules: targeting G-quadruplex structures with oligonucleotides and their analogues. *Nucleic Acids Res.*, **49**, 6638–6659.
9. Asamitsu,S., Obata,S., Phan,A.T., Hashiya,K., Bando,T. and Sugiyama,H. (2018) Simultaneous binding of hybrid molecules constructed with dual DNA-binding components to a G-quadruplex and its proximal duplex. *Chem.*, **24**, 4428–4435.
10. Cadoni,E., De Paepe,L., Colpaert,G., Tack,R., Waegeman,D., Manicardi,A. and Madder,A. (2023) A red light-triggered chemical tool for sequence-specific alkylation of G-quadruplex and I-motif DNA. *Nucleic Acids Res.*, **51**, 4112–4125.
11. Kumar,N., Patowary,A., Sivasubbu,S., Petersen,M. and Maiti,S. (2008) Silencing c-MYC expression by targeting quadruplex in P1 promoter using locked nucleic acid trap. *Biochemistry*, **47**, 13179–13188.
12. Chambers,V.S., Marsico,G., Boutell,J.M., Di Antonio,M., Smith,G.P. and Balasubramanian,S. (2015) High-throughput sequencing of DNA G-quadruplex structures in the human genome. *Nat. Biotech*, **33**, 877–881.
13. Dervan,P.B. and Burli,R.W. (1999) Sequence-specific DNA recognition by polyamides. *Curr. Opin. Chem. Biol.*, **3**, 688–693.
14. White,S., Szewczyk,J.W., Turner,J.M., Baird,E.E. and Dervan,P.B. (1998) Recognition of the four Watson-Crick base pairs in the DNA minor groove by synthetic ligands. *Nature*, **391**, 468–471.
15. Muller,S., Sanders,D.A., Di Antonio,M., Matsis,S., Riou,J.F., Rodriguez,R. and Balasubramanian,S. (2012) Pyridostatin analogues promote telomere dysfunction and long-term growth inhibition in human cancer cells. *Org. Biomol. Chem.*, **10**, 6537–6546.
16. Palumbo,S.L., Ebbinghaus,S.W. and Hurley,L.H. (2009) Formation of a unique end-to-end stacked pair of G-quadruplexes in the hTERT core promoter with implications for inhibition of telomerase by G-quadruplex-interactive ligands. *J. Am. Chem. Soc.*, **131**, 10878–10891.
17. Yu,Z., Gaerig,V., Cui,Y., Kang,H., Gokhale,V., Zhao,Y., Hurley,L.H. and Mao,H. (2012) Tertiary DNA structure in the single-stranded hTERT promoter fragment unfolds and refolds by parallel pathways via cooperative or sequential events. *J. Am. Chem. Soc.*, **134**, 5157–5164.
18. Song,J.H., Kang,H.-J., Luevano,L.A., Gokhale,V., Wu,K., Pandey,R., Sherry Chow,H.H., Hurley,L.H. and Kraft,A.S. (2019) Small-molecule-targeting hairpin loop of hTERT promoter G-quadruplex induces cancer cell death. *Cell Chem. Biol.*, **26**, 1110–1121.
19. Monsen,R.C., DeLeeuw,L., Dean,W.L., Gray,R.D., Sabo,T.M., Chakravarthy,S., Chaires,J.B. and Trent,J.O. (2020) The hTERT core promoter forms three parallel G-quadruplexes. *Nucleic Acids Res.*, **48**, 5720–5734.
20. Long,W., Zheng,B.-X., Huang,X.-H., She,M.-T., Liu,A.-L., Zhang,K., Wong,W.-L. and Lu,Y.-J. (2021) Molecular recognition and imaging of human telomeric G-quadruplex DNA in live cells: a systematic advancement of thiazole orange scaffold to enhance binding specificity and inhibition of gene expression. *J. Med. Chem.*, **64**, 2125–2138.
21. Asamitsu,S., Shioda,N. and Sugiyama,H. (2019) Switching off cancer-causing telomerase using small molecules. *Cell Chem. Biol.*, **26**, 1045–1047.
22. Tijerina,P., Mohr,S. and Russell,R. (2007) DMS footprinting of structured RNAs and RNA–protein complexes. *Nat. Protoc.*, **2**, 2608–2623.
23. Selvam,S., Koirala,D., Yu,Z. and Mao,H. (2014) Quantification of topological coupling between DNA superhelicity and G-quadruplex formation. *J. Am. Chem. Soc.*, **136**, 13967–13970.
24. Li,P.-T., Wang,Z.-F., Chu,I.T., Kuan,Y.-M., Li,M.-H., Huang,M.-C., Chiang,P.-C., Chang,T.-C. and Chen,C.-T. (2017) Expression of the human telomerase reverse transcriptase gene is modulated by quadruplex formation in its first exon due to DNA methylation. *J. Biol. Chem.*, **292**, 20859–20870.
25. Mandal,S., Kawamoto,Y., Yue,Z., Hashiya,K., Cui,Y., Bando,T., Pandey,S., Hoque,M.E., Hossain,M.A., Sugiyama,H., *et al.* (2019) Submolecular dissection reveals strong and specific binding of polyamide–pyridostatin conjugates to human telomere interface. *Nucleic Acids Res.*, **47**, 3295–3305.
26. Mao,H. and Luchette,P. (2008) An integrated laser-tweezers instrument for microanalysis of individual protein aggregates. *Sens. Actuators, B*, **129**, 764–771.
27. Pokhrel,P., Sasaki,S., Hu,C., Karna,D., Pandey,S., Ma,Y., Nagasawa,K. and Mao,H. (2022) Single-molecule displacement assay reveals strong binding of polyvalent dendrimer ligands to telomeric G-quadruplex. *Anal. Biochem.*, **649**, 114693.
28. Baumann,C.G., Smith,S.B., Bloomfield,V.A. and Bustamante,C. (1997) Ionic effects on the elasticity of single DNA molecules. *Proc. Natl. Acad. Sci. U.S.A.*, **94**, 6185–6190.
29. Dhakal,S., Cui,Y., Koirala,D., Ghimire,C., Kushwaha,S., Yu,Z., Yangyuoru,P.M. and Mao,H. (2013) Structural and mechanical properties of individual human telomeric G-quadruplexes in molecularly crowded solutions. *Nucleic Acids Res.*, **41**, 3915–3923.
30. Takahara,P.M., Rosenzweig,A.C., Frederick,C.A. and Lippard,S.J. (1995) Crystal structure of double-stranded DNA containing the major adduct of the anticancer drug cisplatin. *Nature*, **377**, 649–652.
31. Agard,N.J., Prescher,J.A. and Bertozzi,C.R. (2004) A strain-promoted [3 + 2] azide–alkyne cycloaddition for covalent modification of biomolecules in living systems. *J. Am. Chem. Soc.*, **126**, 15046–15047.
32. Hardin,C.C., Watson,T., Corregan,M. and Bailey,C. (1992) Cation-dependent transition between the quadruplex and Watson-Crick hairpin forms of d(CGCG3GCG). *Biochemistry*, **31**, 833–841.

33. Pokhrel,P., Wang,J., Selvam,S., Jonchhe,S., Mandal,S. and Mao,H. (2022) Ensemble force spectroscopy of a G-quadruplex cluster on a single-molecule platform. *Biomacromolecules*, **23**, 4795–4803.
34. Yu,Z. and Mao,H. (2013) Non-B DNA structures show diverse conformations and complex transition kinetics comparable to RNA or proteins — a perspective from mechanical unfolding and refolding experiments. *Chem. Rec.*, **13**, 102–116.
35. Koirala,D., Mashimo,T., Sannohe,Y., Yu,Z., Mao,H. and Sugiyama,H. (2012) Intramolecular folding in three tandem guanine repeats of human telomeric DNA. *Chem. Commun.*, **48**, 2006–2008.
36. Bridges,C.C. (1966) Hierarchical cluster analysis. *Psychol. Rep.*, **18**, 851–854.
37. delVillar-Guerra,R., Trent,J.O. and Chaires,J.B. (2018) G-quadruplex secondary structure obtained from circular dichroism spectroscopy. *Angew. Chem. Int. Ed.*, **57**, 7171–7175.
38. Greenleaf,W.J., Frieda,K.L., Foster,D.A., Woodside,M.T. and Block,S.M. (2008) Direct observation of hierarchical folding in single riboswitch aptamers. *Science*, **319**, 630–633.
39. Koirala,D., Dhakal,S., Ashbridge,B., Sannohe,Y., Rodriguez,R., Sugiyama,H., Balasubramanian,S. and Mao,H. (2011) A single-molecule platform for investigation of interactions between G-quadruplexes and small-molecule ligands. *Nat. Chem.*, **3**, 782–787.
40. Koirala,D., Ghimire,C., Bohrer,C., Sannohe,Y., Sugiyama,H. and Mao,H. (2013) Long-loop G-quadruplexes are misfolded population minorities with fast transition kinetics in human telomeric sequences. *J. Am. Chem. Soc.*, **135**, 2235–2241.
41. Meier,J.L., Montgomery,D.C. and Dervan,P.B. (2012) Enhancing the cellular uptake of Py–Im polyamides through next-generation aryl turns. *Nucleic Acids Res.*, **40**, 2345–2356.
42. Teuscher,K.B., Zhang,M. and Ji,H. (2017) A versatile method to determine the cellular bioavailability of small-molecule inhibitors. *J. Med. Chem.*, **60**, 157–169.

Received: March 24, 2023. **Revised:** July 9, 2024. **Editorial Decision:** August 15, 2024. **Accepted:** August 20, 2024